Kim, Y.M.; Mendis, C.; Sasaki, T.; Letzig, D.; Pyczak, F.; Hono, K.; Yi, S.:
Static recrystallization behaviour of cold rolled Mg-Zn-Y alloy and role of solute segregation in microstructure evolution
In: Scripta Materialia (2017) Elsevier

DOI: 10.1016/j.scriptamat.2017.04.001

Static recrystallization behaviour of cold rolled Mg-Zn-Y alloy and role of solute segregation in microstructure evolution

Young Min Kim[1], Chamini Mendis[1,2], Taisuke Sasaki[3], Dietmar Letzig[4], Florian Pyczak[4], Kazuhiro Hono[3], Sangbong Yi[4]*

1. Korea Institute of Materials Science, 797 Changwondaero, Changwon, 51508, Korea.
2. Brunel Centre for Advanced Solidification Technology (BCAST), Brunel University London, Kingston Lane, Uxbridge, United Kingdom.
3. National Institute for Materials Science, 1-2-1 Sengen Tsukuba, 305-0047, Japan.
4. Institute of Materials Research, Helmholtz-Zentrum Geesthacht, Max-Planck-Str. 1, 21502, Geesthacht, Germany

Abstract

We examined the microstructure and texture evolution during the recrystallization annealing of cold rolled Mg-1Y and Mg-0.2Zn-1Y alloys. At the early annealing stage, new grains are nucleated on sub-units with 200-300 nm surrounded by dislocation walls within shear bands. The Zn and Y addition reduced the stacking fault energy which results in the high activity of non-basal deformation mechanisms and formation of segregation zones along the stacking faults. This causes the orientation of recrystallization nuclei to be effectively retained so that the texture weakens during the recrystallization without reducing the basal pole split into the sheet transverse direction.

Keywords:

Magnesium alloys; Shear band; Recrystallization; Stacking faults; Texture

The addition of rare earth elements (REE) or Ca into Mg and its alloys leads to a weakening of texture with the maximum orientation locating at off-basal component. A number of studies reported that the texture weakening results in a substantial improvement of sheet formability and ductility at low temperature [1 - 5]. Various mechanisms have been proposed to explain the texture weakening in such alloys. For example, higher activity of non-basal type dislocations, twinning and a homogeneous shear banding deformation have been reported from the point of deformation [6, 7], while recrystallization nucleation triggered at twin and/or shear band, particle stimulated nucleation and drag effect of solute and particles on grain boundary motion have been investigated with respect to the recrystallization [8 - 11]. It is still controversial as to which of these mechanisms play a dominant role in weakening the texture and how the different mechanisms interact on each other. The difficulties associated with experimental investigations on the above questions are mainly due to Mg alloys needing to be deformed at elevated temperatures. Thus, the resulting microstructure and

texture are affected by dynamic recovery and dynamic recrystallization, which occurs during hot processing of Mg alloys, so that the influence of deformation and recrystallization mechanisms on the resulting microstructures are difficult to be separately analysed. The texture randomisation with the basal pole split into the sheet transverse direction (TD) has been observed during the recrystallization annealing of Zn containing Mg-REE ternary alloy sheets and Mg-Zn-Ca alloys [11, 13 - 15]. Even though the transition of the main texture component to the split basal pole to TD has been phenomenologically reported and this type of texture is very beneficial for the formability of the sheets, the influence of the Zn addition on the texture evolution of the Mg-REE alloys is not fully understood. The present study contributes to a basic understanding of the role of the REE, especially in combination with Zn addition, to the microstructure and texture evolution during recrystallization processes of cold rolled sheets from the nucleation to grain growth.

Two Y containing Mg alloys, Mg – 1.0 wt.% Y (W1) and Mg – 0.9 wt.% Y – 0.2 wt.% Zn (ZW01), were cast into steel mould under Ar + SF_6 atmosphere. After homogenisation at 500 °C for 12 hrs, slabs of a thickness of 20 mm were machined from the as-cast alloys. The slabs were rolled to a thickness of 2 mm using 12 passes with intermediated annealing at 450 °C. Then, the hot rolled sheets were rolled to a thickness of 1 mm at room temperature, which corresponds to the deformation degree ($\varphi = -\ln\ (h_{before}\ / h_{after})$) of 0.69 subjected by cold rolling. The samples were recrystallization annealed at 350 °C and held for 1 to 120 min under atmospheric conditions using an air recirculating furnace. The global texture of the rolled and annealed sheets was investigated using X-ray diffraction (Panalytical, at 40kV and 40 mA), where 6 incomplete pole figures of {10.0}, (00.2), {10.1}, {10.2}, {11.0} and {10.3} planes were collected and the complete pole figures were calculated using MTEX software [12]. Samples for transmission electron microscopy (TEM) were prepared with twin jet electro-polishing in a solution of 1.5 vol. % perchloric acid in ethanol at -45 ^{o}C and a voltage of 50 V using a Fishione twin jet electopolisher. The analytical TEM was conducted with a Phillips CM 200 (FEI) TEM operating at 200kV. The atomic resolution high angle annular dark field scanning transmission electron microscopy (HAADF-STEM) was conducted on a FEI Titan G2 80-200 TEM operating at 200kV. In order to ensure a cleanliness of the samples for HAADF-STEM, the TEM samples were polished with a Gatan precision ion polishing system (PIPS), Gatan Model 691 at 2, 1 and 0.3 kV for 15 min.

The optical micrographs of the W1 and ZW01 sheets after cold rolling and recrystallization annealing are presented in Fig. 1 (a). A large amount of the shear bands, inclined about 35° to the sheet rolling direction (RD), developed in the cold rolled W1 and ZW01 sheets to cover the majority of the analysed volume. The matrix grains containing twins are elongated along the RD and surrounded by shear bands. After the annealing at 350 °C for 10 min the W1 alloy show significant amount of recrystallization, while the ZW01 alloy has a partially recrystallized structure at former shear bands. The average size of the recrystallized globular grains in the W1 and ZW01 alloys is 6.2 μm and 1.5 μm

respectively. In addition, the area fraction of the recrystallized, strain-free grains, measured by electron backscatter diffraction (EBSD), is 0.57 and 0.29 in the W1 and ZW01 alloys respectively. The highly retarded recrystallization and grain growth in the ZW01 alloy result in the average grain size of 4.5 μm after the annealing for 60 min, which is half that of the W1 alloy (9.0 μm). The as-rolled W1 sheet shows a strong basal-type texture with the max (0002) pole density P_{max} of 17.0 m.r.d., while the as-rolled ZW01 sheet has a split of basal pole toward the RD together with a broadening in the TD with the P_{max} of 5.6 m.r.d., Fig. 1 (b). During the annealing at 350 °C the W1 sheet maintains the basal-type texture, while the texture intensity decreases with the beginning of recrystallization annealing up to 10 min and then the texture strengthens slightly with further annealing. In contrast, a gradual texture weakening is observed during the annealing of the ZW01 sheet. Interestingly, the latter shows a transition of the main texture component from the basal pole split in the RD during the initial recrystallization to the basal pole tilted about 55° toward the TD after about 30 min annealing. The microstructure evolution during recrystallization annealing of the W1 and ZW01 alloys was investigated using TEM with a focus on the influence of Zn on Mg-REE alloys on the texture development.

Microstructural features at the shear bands in cold rolled ZW01 sheet, Fig 2, show a severely deformed structure with a high dislocation density in the shear bands in the vicinity of relatively un-deformed matrix grains, Fig. 2 (a). The enlarged image of the shear band shows that they contain aligned micro-band structures, Fig. 2 (b). The formation of cell structure with the size of 200 ~ 300 nm, which is divided by high-density of dislocations accumulated inside contraction twins, is observed within the micro-bands. The selected area electron diffraction (SAED) pattern from the area corresponding to Fig. 2 (b) indicates that the {1-101} reflections are shared commonly between different micro-bands, Fig. 2 (c). This is consistent with the twinning plane of $\{10\bar{1}1\}$ $<10\bar{1}\bar{2}>$ contraction twins. For guidance, the 1-101 reflections and the diffraction patterns from different micro-bands are marked on the SAED pattern. Furthermore, Fig. 2 (b) reveals that high-density dislocations accumulate within the twins and their boundaries are not straight but curved. The curved twin boundaries can result from the interaction between gliding dislocations inside twins and twin boundaries by a severe plastic deformation (SPD) during cold rolling and the dislocations accumulation at twin boundaries. Zhang et al. [16] investigated on dislocation-twin boundary interaction in Hadfield steel (X120Mn12), with stacking fault energy 48 mJ/m^2, during a SPD process. Similar to the observations in the present study, they found the transition of twin boundary morphology from flat to rough as SPD continues, and the curved twin boundaries become high angle grain boundaries leading to the nanocrystallization of Hadfield steel. It should be noted that the microstructure of the cold rolled W1 sheet (not shown in the present paper) is very similar to that in the ZW01 sheet with regards to the shear bands and its structure.

Transmission electron micrographs in Fig. 3 are from samples heat-treated at 350 °C for 3 min and 350 °C for 1 min for ZW01 and W1 cold rolled sheets, respectively. Due to the large difference in the recrystallization kinetics, a comparable microstructure was found after a shorter annealing of the W1 than the ZW01 alloy sheet. The SAED pattern from the areas in the ZW01 sheet marked A and B in Fig. 3 (a) reveals the $\{10\bar{1}1\}$ twin relationship between the micro-bands. The $\{1\bar{1}01\}$ reflections from two adjacent micro-bands, e.g. SAED pattern from the area B, are approximately 3° away from the ideal position due to the interaction of dislocations with twin boundaries. In the ZW01 and W1 sheets the formation of some strain-free grains is observed at the micro-bands, the dashed lines and the arrows in Fig. 3 (a) and (c). The nucleation of new grains by static recrystallization is triggered by the formation of 100 ~ 300 nm cell structures at the shear bands, which are recognized from a change in image contrast within micro-bands. That is, the cell boundaries which form by accumulated dislocations during cold rolling turn to high angle boundaries by rotational rearrangements. The crystallographic features of the dislocations at the shear band are hard to be identified in the as-rolled sheets due to the overall high degree of deformation. In contrast the dense dislocation arrays on prismatic and pyramidal planes are observed during the early stages of recrystallization within the cell structures developed at the previous shear bands in the ZW01 and W1 alloys, e.g. Fig. 3 (c). It can be deduced from the rotation recrystallization that the orientations of the recrystallization nuclei are controlled by the dominantly operating slip systems in such a way that a more randomised orientation distribution develops with the basal pole splits into the RD as well as the TD from highly accumulated dislocations.

Figs. 4 (a) and (b) illustrate the grains recrystallized at the former shear bands after heat treatment of the W1 and ZW01 alloys at 350 °C for 10 min, respectively. At the intermediate recrystallization stage, i.e. a mixed microstructure between strain-free grains nucleated at the former shear bands and matrix grains retaining the deformed structure with internal orientation gradients, there are clear differences in the microstructural evolution between the W1 and ZW01. The W1 alloy has higher recrystallization kinetics compared with the ZW01 alloy in terms of the nucleation as well as growth of new grains. Moreover, linear structures forming on (0001) planes of Mg were observed in ZW01 alloy when viewed along $<2\bar{1}\bar{1}0>$ zone axis and were identified as stacking faults (SF) through large angle tilting. These SFs are stable and are observed after the heat treatment at 350 °C for 60 min, Fig. 4(c). However, the W1 alloy samples examined in the present study did not show the formation of SFs during heat treatments, Fig. 4 (a). The HAADF-STEM image of the SFs in the ZW01 alloy sheet after heat treatment for 10 min in a region containing SFs is illustrated in Fig. 4 (d). The bright columns of atoms correspond to SFs observed in the Fig 4 (b). The Zn and Y atoms appear brighter compared with Mg atoms due to the atomic number contrast [17]. The bright contrast associated

with the SF shows the localised segregation of Zn and Y to stacking faults. The atomic segregation was approximately 3 atomic layers in thickness.

The reduction of SF energy by the addition of REE into Mg alloy has been reported in experimental and numerical investigations [18, 19]. Some investigations based on simulations showed that the SF energy decreases dramatically with the simultaneous addition of Y and Zn in comparison to the singular addition of Y [18]. The long ranged stacking order structure of 14H-type formation was observed in Mg - 1at.% Zn – 2 at.% Y triggered mainly due to the enrichment of Zn and Y atoms on the basal planes [17]. The results from this study indicate that the ternary addition of small amount of Zn, even less than 1 wt.%, into W1 alloy results in a significant decrease in the SF energy and promotes SF formation during recrystallization annealing. The reduced SF energy in the REE containing Mg alloys leads to an increased activation of non-basal deformation mode, which is supported by the experimental observation of this study, i.e. dense arrays of micro-bands having $\{10\bar{1}1\}$ twin orientation and the high density of prismatic and pyramidal dislocations, Figs. 2 and 3. The lowering of SF energy leads also to changes in the recrystallization kinetics, e.g. retardation in the recovery process due to difficulties in cross slip and climb of dislocations. Additionally, the segregation of heavy alloying elements to SFs during the annealing, which is a unique microstructural feature observed in the ZW01 alloy, plays an important role on the deformation mechanism and the microstructure evolution. It can be expected that the segregation along the (0001) planes hinders the dislocation glide on basal plane. Due to the hindrance of basal dislocations glide it can be inferred that the prismatic and pyramidal dislocation glide contribute to the deformation, e.g. during a deformation process of the annealed ZW01 alloy sheet. The pinning effect on the boundary motion due to solute segregation at twin and grain boundaries has been reported previously [11, 20]. The segregation of Zn and Y atoms at SFs observed in the present study contributes to the reduction in the boundary movements, which agrees with the slower recrystallization kinetics of ZW01 compared with W1 alloy sheet. Given that the boundary movement against the segregation plane, i.e. (0001) plane, is impeded more than in other directions, the grain growth occurs in an anisotropic way so that ellipsoid shape grains with a longer axis parallel to the SFs form during the recrystallization. In fact, a development of ellipsoidal grains having its minor axis in [0001] direction and a stepwise grain boundary is observed in the ZW01 alloy annealed for 60 min, Fig. 4(c). The texture developments of W1 and ZW01 sheets are understood in relation with the above mentioned microstructural features. At the early stages of annealing, the recrystallization process triggered at the shear bands leads to a decrease in sharpness of texture in the both alloys. In the W1 alloy, deformation energy is released relatively rapid during recrystallization process and subsequently the texture strengthens again with the accompanying grain growth. In contrast, a significant retardation of the recovery and boundary motion is observed in the ZW01 alloy, as a result of significantly reduced SF energy and subsequent

segregation of Zn and Y at SFs. Therefore, recrystallization nuclei which are triggered at shear bands with more randomised orientation distribution can grow without being consumed by the energetically beneficial larger volume grains, e.g. matrix grains neighbouring shear bands. With the equivalent growth of the recrystallization nuclei, the global texture weakens without a dominant growth of the grains having a basal-type orientation. As the orientations of the nuclei result from the twinning as well as prismatic and pyramidal dislocation glide, the corresponding orientations which also includes the texture component of the basal pole split into the TD are maintained steadily during the recrystallization and grain growth.

In summary, cold rolling Mg-Y alloys led to a formation of homogeneously distributed shear bands consisting of fine micro-bands. Small addition of Zn into Mg-Y alloy results in; (1) significant reduction of stacking fault energy which is lower than that in Mg-Y binary alloy, (2) stacking fault form along (0001) planes during the annealing and subsequently Zn and Y atoms segregate at the stack faults, (3) considerable retardation of recovery and recrystallization process. By the impeded grain growth, the orientation of recrystallization nuclei can be retained more effectively and hence the sharpness of the texture decreased without reduction in the orientation corresponding to the texture component of basal pole split into TD.

Acknowledgements

Financial supports of DFG - German Research Foundation (YI103/1-2) for the research stay of YM Kim at HZG and the NST - National Research Council of Science & Technology (No. CRC-15-06-KIGAM) by the Korea government (MSIP) are gratefully acknowledged. The authors are grateful to Y.K. Shin at HZG for technical supports.

References

[1] T. Al-Samman, X. Li, Mater. Sci. Eng. A, A528 (2011) 3809-3822.

[2] K. Hantzsche, J. Bohlen, J. Wendt, K. U. Kainer, S. Yi, D. Letzig, Scripta Mater., 63 (2010) 725-730.

[3] Y. Chino, M. Kado, M. Mabuchi, Mater. Sci. Eng. A, A494 (2008) 343-349.

[4] S. Yi, J. Bohlen, F. Heinemann, D. Letzig, Acta Mater., 58 (2010) 592-605.

[5] J. Hirsch, T. Al-Samman, Acta Mater., 61 (2013) 818-843.

[6] I. Basu, T. Al-Samman, G. Gottstein, Mater Sci. Eng. A, A579 (2013) 50-56.

[7] N. Stanford, M. Barnett, Mater. Sci. Eng. A, A496 (2008) 399-408.

[8] E.A. Ball, P.B. Prangnell, Scripta Metall. Mater., 31 (1994) 111-116.

[9] T. Al-Samman, Mater. Sci. Eng. A, A560 (2013) 561-566.

[10] J.P. Hadorn, K. Hantzsche, S. Yi, J. Bohlen, D. Letzig, J. A. Wollmershauser, S.R. Agnew, Metall. Mater. Trans. A, 41A (2012) 1347-1362.

[11] Z.R. Zeng, Y.M. Zhu, S.W. Xu, M.Z. Bian, C.H.J. Davies, N. Birbills, J. F. Nie, Acta Mater., 105 (2016) 479-494.

[12] F. Bachmann, R. Hielscher, H. Schaeben, Solid State Phenomena, 160 (2010) 63-68.

[13] I. Basu, T. Al-Samman, Acta Mater., 67 (2014) 116-133.

[14] D.-W. Kim, B.-C. Suh, M.-S. Shim, J.H. Bae, D.H. Kim, Nack J. Kim, Metall. Mater. Trans. A, 44A (2013) 2950-2961.

[15] J. Bohlen., J. Wendt, M. Nienaber, K.U. Kainer, L. Stutz, D. Letzig, Mater. Characterization, 101 (2015) 144-152.

[16] F. Zhang, X. Feng, Z. Yang, J. Kang, T. Wang, Scientific Reports, 5 (2015) 8981.

[17] D. Egusa, E. Abe, Acta Mater., 60 (2012) 166-178.

[18] S. Sandlöbes, M. Friák, S. Zaefferer, A. Dick, S. Yi, D. Letzig, L.-F. Zhu, J. Neugebauer, D. Raabe, Acta Mater., 60 (2012) 3011-3021.

[19] Q. Zhang, L. Fu, T.-W. Fan, B.-Y. Yang, L.-M. Peng, W.-J. Ding, Physica B, 416 (2013) 39-44.

[20] J.F. Nie, Y.M. Zhu, J.Z. Liu, X.Y. Fang, Science, 340 (2013) 957-960.

List of figures

Figure 1.
(a) Optical micrographs at RD-ND longitudinal plane and (b) recalculated (0002) pole figures of the W1 and ZW01 sheets after cold rolling and subsequent annealing for 10 min and 60 min at 350°C (m.r.d. = multiple random degree).

Figure 2.
(a) Transmission electron micrograph of the cold rolled ZW01 sheet showing shear band 'SB' in the vicinity of matrix grain 'M'. (b) Magnified view inside shear band and (c) selected area diffraction pattern taken from the selected area of (b). For guidance the SAED pattern of the micro-bands are marked by hexagons in different colours.

Figure 3.
TEM micrographs at the early recrystallization stage of (a) ZW01 sheet annealed at 350 °C x 3 min. (b) Dislocation structures and (c) formation of a strain-free grains inside micro-bands observed in the W1 sheet annealed at 350 °C x 1 min. Note that the SAED of the area 'B' shows a similar orientation relationship with that shown in Fig. 2 (c).

Figure 4.
TEM micrographs of recrystallized grains triggered at the formal shear bands of (a) W1 sheet and (b) ZW01 sheet after 350 °C x 10 min annealing. (c) ZW01 sheet after 350 °C x 60 min annealing. (d) HAADF-STEM image in the vicinity of grain boundary of recrystallized grain of ZW01 sheet annealed at 350 °C x 10 min, showing the local segregation of heavy elements at the stacking faults.

Figure 1.
(a) Optical micrographs at RD-ND longitudinal plane and (b) recalculated (0002) pole figures of the W1 and ZW01 sheets after cold rolling and subsequent annealing for 10 min and 60 min at 350°C (m.r.d. = multiple random degree).

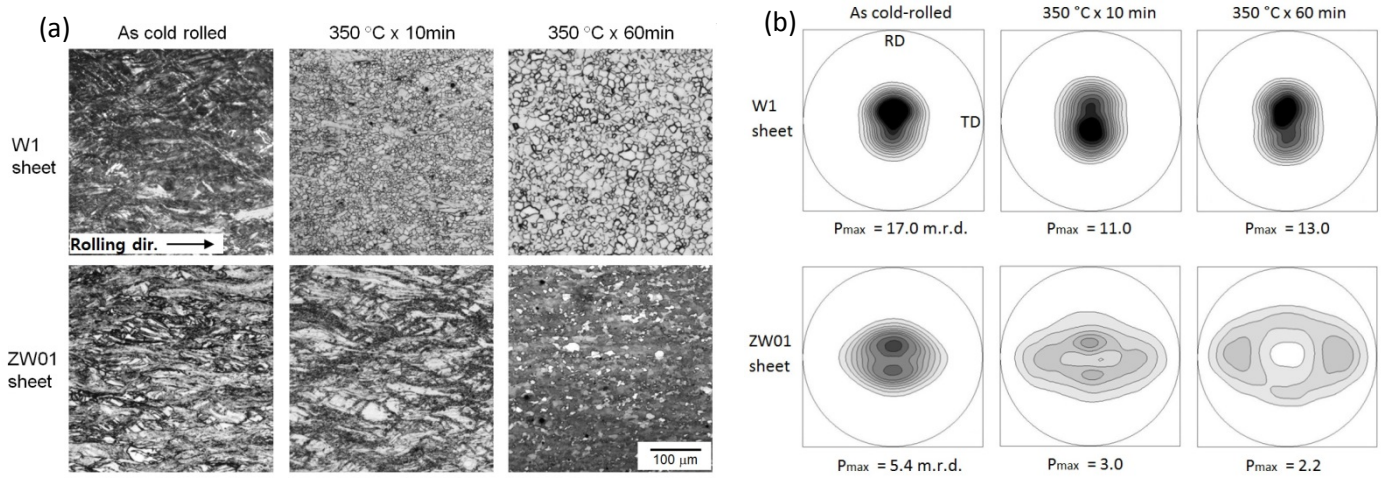

Figure 2.
(a) Transmission electron micrograph of the cold rolled ZW01 sheet showing shear band 'SB' in the vicinity of matrix grain 'M'. (b) Magnified view inside shear band and (c) selected area diffraction pattern taken from the selected area of (b). For guidance the SAED pattern of the micro-bands are marked by hexagons in different colours.

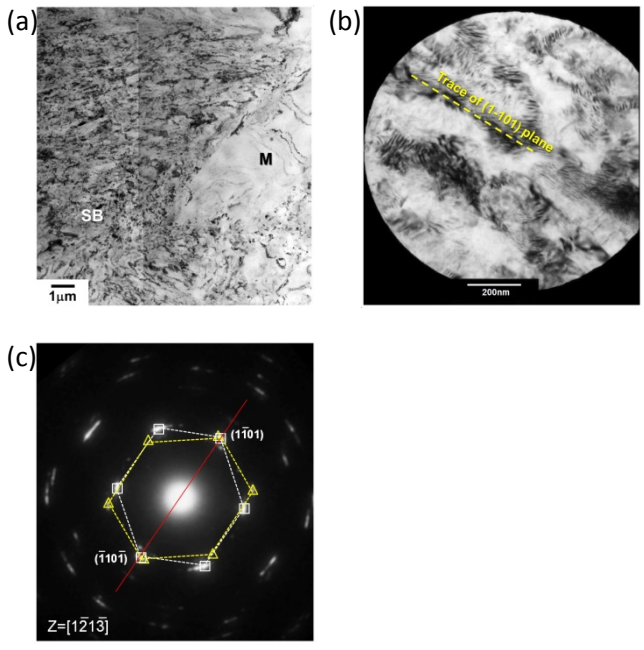

Figure 3.
TEM micrographs at the early recrystallization stage of (a) ZW01 sheet annealed at 350 °C x 3 min. (b) Dislocation structures and (c) formation of a strain-free grains inside micro-bands observed in the W1 sheet annealed at 350 °C x 1 min. Note that the SAED of the area 'B' shows a similar orientation relationship with that shown in Fig. 2 (c).

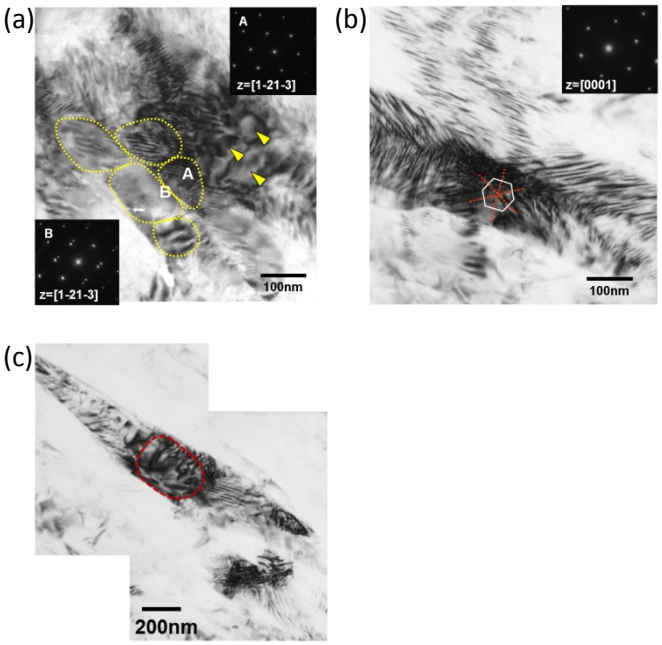

Figure 4.

TEM micrographs of recrystallized grains triggered at the formal shear bands of (a) W1 sheet and (b) ZW01 sheet after 350 °C x 10 min annealing. (c) ZW01 sheet after 350 °C x 60 min annealing. (d) HAADF-STEM image in the vicinity of grain boundary of recrystallized grain of ZW01 sheet annealed at 350 °C x 10 min, showing the local segregation of heavy elements at the stacking faults.